Hindawi
Advances in Materials Science and Engineering
Volume 2019, Article ID 8930134, 16 pages
https://doi.org/10.1155/2019/8930134

Research Article

Research on Multipass Hot Spinning Process Technology of AZ80 Magnesium Alloy Shell

Wei Liang[1], **Lin Guan**[2], **Qiongying Lv**[1] and **Zhigang Xing**[1]

[1]*College of Mechanical and Electrical Engineering, Changchun University of Science and Technology, Changchun, Jilin, China*
[2]*College of Foreign Languages, Changchun University of Science and Technology, Changchun, Jilin, China*

Correspondence should be addressed to Lin Guan; guanlin@cust.edu.cn

Received 7 May 2019; Accepted 18 September 2019; Published 30 November 2019

Academic Editor: Guoqiang Xie

Combined with finite element numerical simulation analysis, the hot-spin forming technology of cylindrical AZ80 magnesium alloy parts was studied in the paper. The multipass hot-spin forming of magnesium alloy shell parts was simulated by the ABAQUS software to analyze the stress and strain distribution and change during spinning for the preliminary test process parameters in the magnesium alloy spinning test. Then, the process parameters were optimized during the hot spinning test, especially the matching relationship between temperature parameter and thinning rate parameter, and the hot spinning magnesium alloy shell parts with the expected technical specifications were finished.

1. Introduction

Magnesium alloy is so far the lightest structural metal found in the world with its density being 1.7~1.9 g/cm^3. With the advantages of low density, high strength, good thermal conductivity, strong shock resistance, anti-electromagnetic interference, good shielding performance, and reusability, magnesium alloy has become one of the "youngest" structural metal materials [1, 2]. However, the application of magnesium alloys is limited to a large extent because of their close-packed hexagonal structure with few slip systems and poor plasticity at room temperature [3–5]. At present, more than 80% of the world's magnesium alloy parts are produced with the casting process, which often results in coarse grain structure, insufficient mechanical properties, and defects of shrinkage [6].

In order to improve the forming process of magnesium alloys and extend the application of magnesium alloys, the plastic forming process mode of magnesium alloys including extrusion and spin forming is gradually applied [7]. With the features of refining magnesium alloy grains during the spinning process, improving the tensile strength and yield strength performance, and toughening the magnesium alloy material, the spinning process is supposed to be the major processing means for magnesium alloy thin-walled shell parts in the future [8–10]. In the spinning process, heating and spinning must be carried out, and the key technologies and difficulties lie in the accurate determination of the spinning heating temperature and its control range according to the process parameters such as thinning rate and feed rate, especially for cylindrical parts with large length-diameter ratio. In this paper, the ABAQUS software is used to simulate the process parameters in multipass heating and spinning of magnesium alloy shell parts to provide the feasible experimental parameters, which are then verified and optimized through the spinning test. The study examines the feasibility of the multipass hot spinning of magnesium alloy shell parts as well as the precision control range and matching relationship of the relevant process parameters for further data reference.

2. Simulation Analysis of Hot-Spin Forming of Cylindrical Magnesium Alloy Parts

The strong spinning of the cylindrical part (generally called flow spinning) is a typical partial loading, point-by-point deformation forming process, which has the advantages of labor saving, material saving, and flexibility. It is a metal near

net forming method, which can produce a thin-walled, high-precision cylindrical parts [11]. The test piece of the magnesium alloy cylindrical part shell is a bottomed cylindrical part, which was previously formed by a positive rotation method [12]. The main process parameters affecting the spinning quality of the cylindrical parts are thinning rate, feed rate f, spindle speed n, spinning temperature, rotor structure, etc. The main purpose of the cylindrical part spinning simulation is to analyze the influence of process parameters on spinning process, thereby optimizing the process parameters [13, 14].

2.1. Spinning Process and Parameters of Cylindrical Magnesium Alloy Parts. As is shown in Figure 1, the target grade of magnesium alloy tubular test specimen is AZ80, the inner diameter of the part size is φ180 mm, the wall thickness is ≤10 mm, and the difference of circumferential wall thickness is not more than 0.2 mm. The wall thickness of the blank to be tested is 30 mm and is reduced to 10 mm in the spinning forming process with the thinning rate being 66.7%, which exceeds the thinning rate limit of the spin forming of the magnesium alloy. The calculation formula is shown in formula 1. Therefore, multipass spin forming is employed in the spinning process. Considering the data of the AZ80 magnesium alloy in T4 state with the thinning rate limit being 37.8% [15], we set 4 forming passes, with the thinning rates being 23%, 26%, 29%, and 25% respectively.

$$\psi_t = \frac{\left(t_0 - t_f\right)}{t_0} \times 100\%. \quad (1)$$

The magnesium alloy tubular part forming employs a two-wheel positive rotation, and the rotating wheel structure is a double-cone surface rotating wheel with a forming section and an exciting section. The structure of the rotating wheels is similar, but the forming angles of the rotating wheels are different. The shapes of the rotating wheels are shown in Figure 2. The front wheel forming angle is 21°, the rear wheel forming angle is 25°, and the exit angles are both 25°. The round radii of the wheels are the same, the value of R_ρ is 6 mm, and the 10 mm simulation optimization is suitable for the radii of the wheels of the cylindrical magnesium alloy pieces.

There is a certain relationship between the offset and the amount of the reduction of rotating wheels in the stagger spinning of the cylindrical parts [16]. The offset is represented by C, the forming angle of the rotating wheels is α_ρ, and the difference between the amount of the reduction of two front and rear wheels is ΔT. The limit state is shown in Figure 3 for the condition when the front and rear wheels simultaneously contact the blank while spinning, and the difference between the front wheel and the rear wheel in reduction ΔT is equal to $C \times tg\alpha_\rho$, that is, $\Delta T = C \times tg\alpha_\rho$, whereas the front wheel will not work when the difference ΔT is greater than $C \times tg\alpha_\rho$, that is, $\Delta T > C \times tg\alpha_\rho$. Therefore, when the front and rear wheels are the same in structure, the difference ΔT between the front wheel and rear wheel in reduction must be less than or equal to $C \times tg\alpha_\rho$. Generally speaking, the forming angle of the rear wheel of the cylindrical part should be slightly larger than that of the front wheel [17, 18]. Assuming that the forming angles of each of the rotating wheels are the same and the front wheel forming angle of the first contact blank α_ρ is 21, the offset C satisfies the condition $\Delta T \le C \times tg\alpha_\rho$ in order for the rotating wheels to be in sequential contact with the blank. The amount of reduction affects the value of ΔT, which results in a difference in offset.

Generally speaking, metals can be processed by cold spinning, but magnesium alloys with poor plasticity must be

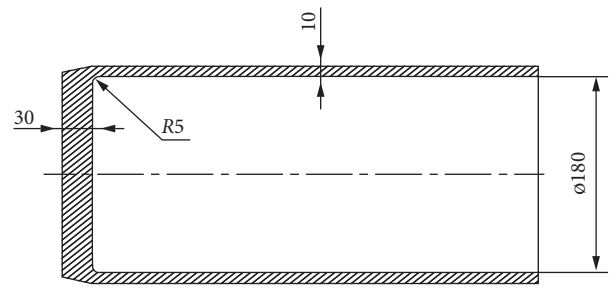

Figure 1: Target sample size.

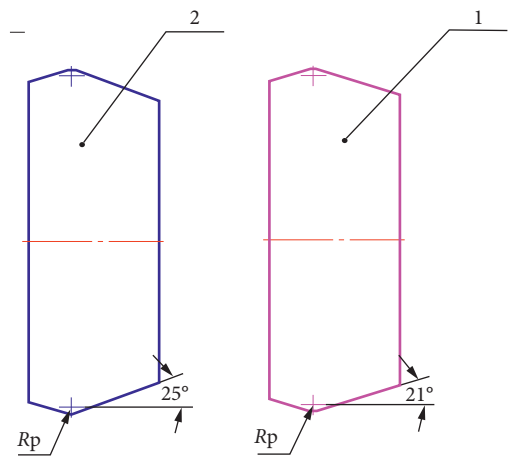

Figure 2: Shape and size of rotary wheels. 1, front wheel; 2, rear wheel.

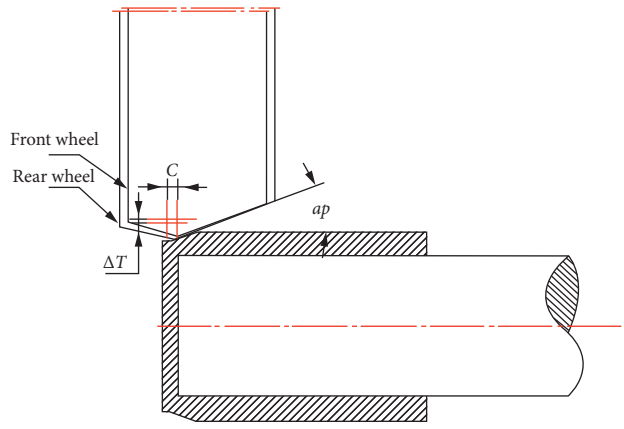

Figure 3: Offset analysis of the wheels.

subjected to hot spinning. The purpose of heating is to improve the spin ability of the material and reduce its deformation resistance. The upper limit of the heating temperature is supposed to be lower than the phase transition temperature of Ac1 to prevent recrystallization [19, 20]. The lower limit is supposed to be higher than the brittle zone of the material. In our experiment, the spinning temperature was set to 250°C, 300°C, 350°C, and 400°C in four groups, and we comparatively analyzed the stress and strain curves at different temperatures. According to the above data, the corresponding parameters in the simulation model are summarized in Table 1, and the basic process parameters to be used in spinning simulation are shown in Table 2.

2.2. Establishment of the Spinning Simulation Model for Cylindrical Magnesium Alloy Parts

2.2.1. Construction of Simulation Geometry Model and Mesh Division. The model used in this paper is established in ABAQUS software. The established finite element model is shown in Figure 4. The wall thickness of the material is 30 mm, the length is 220 mm, and the 2 rotors are symmetrically placed at 180°.

The blank is a three-dimensional deformable solid and is meshed by an eight-node linear hexahedron C3D8R unit; the spiral wheel and the core mold are three-dimensional discrete rigid shells, and the mesh type is a four-node three-dimensional bilinear rigid quadrilateral R3D4. In order to speed up the simulation, a step-by-step modeling calculation method is adopted. At the same time, to facilitate the model establishment and mesh division, we simplified the model and made the wall thickness of each pass consistently the same.

2.2.2. Material Model. In order to predict the metal forming process, it is necessary to previously determine the quantitative relationship between the deformation thermodynamic parameters of the material under the condition of hot working deformation. The flow law or constitutive equation is the basic information of the deformation properties of materials, which shows the dependencies among flow stress and strain, strain rates, and temperatures. We conducted a strict isothermal compression experiment, in which the exact stress-strain curves of magnesium alloys at different temperatures and strain rates were obtained to fit the mathematical model of hot-spin forming of magnesium alloys. The curves are supposed to be applied to the finite element simulation to scientifically formulate the actual production process and optimize process parameters. The mechanical properties of magnesium alloys are shown in Table 3. For the compression test of the magnesium alloy, the accurate stress-strain curve with a strain rate of $0.1\,s^{-1}$ is shown in Figure 5.

2.2.3. Contact and Boundary Conditions

(1) Contact. The friction involved in the spinning simulation of the barrel body mainly includes the friction between the blank and the core mold and the friction between the blank and the rotating wheel. Since the rotating wheel rotates around its own axis during feed motion, there is not only sliding friction in the contact zone but also rolling friction, which exhibits a nonlinear characteristic. In order to simplify the simulation process, this simulation assumes a friction coefficient of 0.

(2) Boundary Conditions. In the spinning experiment, the main shaft drives the blank and the mandrel to make a rotary motion together. The rotating wheel performs the axial feed motion and applies a certain rotational pressure to the blank for processing. However, in practice, such motion patterns and processes are difficult to implement in the finite element numerical simulation process. The reason is that the simulation with a larger mass amplification factor can increase the corresponding speed in order to save the simulation time, for example, if the mass is amplified by 10000 times, the speed can be increased by 100 times. If the equipment is operated at a speed of 100 times the actual value, the increase in the speed of the moment of inertia of the blank will result in the moment when the blank in contact with the rotating wheel in high-speed operation is damaged. Therefore, the relative motion is adopted. Assuming that the mandrel and the blank are stationary, the rotating wheel performs simultaneous rotational motion and axial movement along the surface of the blank, and the force of the rotating wheel acts on the blank to result in plastic deformation of the blank.

The blank is fixed to the mandrel, and the rotating wheel rotates along the circumferential direction of the blank and feeds along the axis direction. The parameter setting adopts the speed control mode to set the feed speed and rotate speed.

2.2.4. Grid Meshing. The spinning simulation of the magnesium alloy cylindrical parts consists of three simulation target models, which are used to simulate the blank material, the spinning wheel, and the mandrel model. In the simulation process, the blank material model is divided into 10384 cells with the size of 30 mm × 220 mm. The grid form is shown in Figure 6(a). The wheel model is divided into a 21° wheel and a 25° wheel according to the forming angle. The number of grids is 3024 and 2886, respectively, as shown in Figure 6(b). The mandrel model is divided into 7342 cells, and the corner diameter of the front end of the mandrel is 5 mm, the same as that of the target sample, as shown in Figure 6(c).

2.3. Simulation of Multipass Spinning of Cylindrical Magnesium Alloy Parts.

Spinning of magnesium alloy cylindrical parts from a wall thickness of 30 mm to 10 mm requires a four-pass spinning process. According to the aforementioned performance analysis and spinning process design, the four-pass spinning simulation process parameters are determined as shown in Table 4.

2.3.1. Stress, Strain, and Cross-Sectional Distribution of the First Pass. In the first pass, the thickness of the blank is large, which can be rotated with large reduction. Since the

Table 1: Parameter values of various components in the simulation model.

Parts	Parameters	Symbols	Units	Parameter values
Blank	Thickness of the wall	t_0	mm	30
	Length	L		220
	Inner diameter	R_{in}		180
Rotary wheel	Angle of the front wheel	α_ρ	°	21
	Angle of the rear wheel			25
	Round corner diameter	R_ρ	mm	6, 10
Mandrel	Diameter	φ	mm	180
	Front round corner diameter	r	mm	5

Table 2: Basic process parameters of spinning simulation.

Parameters	Symbols	Units	Parameter values
Main spindle speed	n	r/min	60, 90
Feed rate	f	mm/r	0.7, 1
Total thinning rate	ψ_t	%	66.7
Spinning temperature	T	°	270 ± 10
Reduction of the wheel	C	mm	3, 6

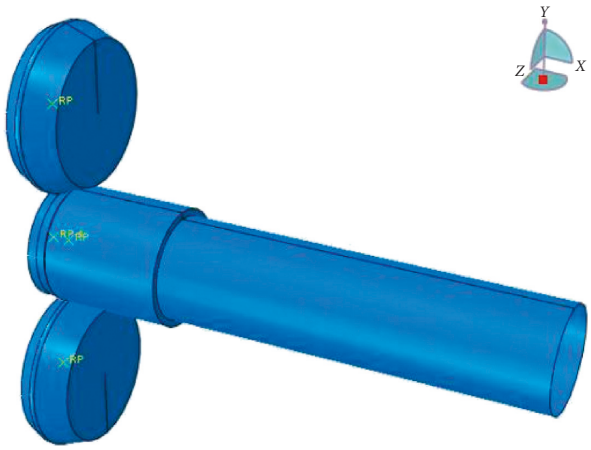

Figure 4: Finite element model.

Table 3: Mechanical properties of magnesium alloys.

Material	Density	Elasticity modulus	Poisson's ratio
Magnesium alloy	1.77 g/cm^3	42 GMPa	0.29

subsequent passes will level the surface of the previous pass, the feed rate can be appropriately increased to improve the production efficiency. The initial selection of the process parameters for the first pass is shown in Table 4. The stress, strain, and cross-sectional distribution are shown in Figures 7 and 8. The maximum value of the spinning stress appears at the contact of the rotating wheel and the blank. The maximum stress during the spinning process is always maintained at about 16.38 MPa. The spinning process is stable, the blank is well applied, and the flange appears at the bottom of the blank, and the local deformation increases (As shown in Figure 7(c) below). There is a bell mouth at the bottom, and the outer metal flows more than the inner metal (Figure 7(d)).

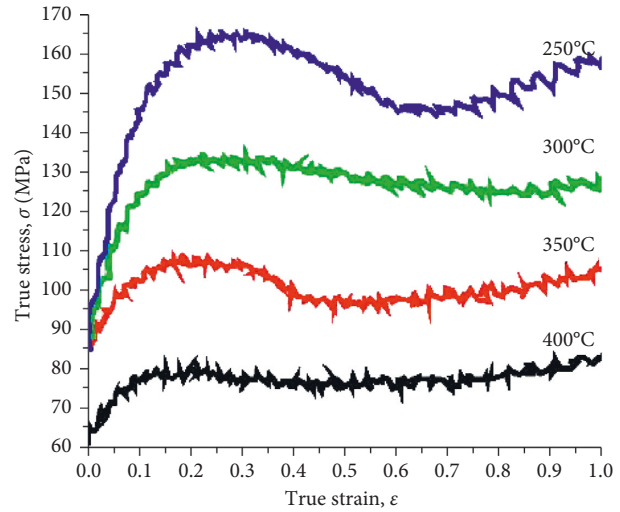

Figure 5: Stress-strain curve with a strain rate of 0.1 s^{-1}.

The equivalent strain distribution of the first pass is shown in Figure 8.

2.3.2. Stress, Strain, and Cross-Sectional Distribution of the Second Pass. The equivalent stress distribution of the second pass of the spinning process is shown in Figure 9. The maximum value of the spinning stress appears at the contact of the rotating wheel and the blank. The maximum stress during the spinning process is always maintained at 16.38 Mpa. The spinning process is stable, and the blank is well applied, while the bottom of it is thinned. When the spinning process is finished, the nonparallelism at the end of the blank increases. The deformation of the spinning process is not uniform, which needs to be compensated by subsequent passes.

The equivalent strain distribution of the second pass of the spinning process is shown in Figure 10.

2.3.3. Stress, Strain, and Cross-Sectional Distribution of the Third Pass. The stress, strain, and cross-sectional distribution of the third pass of the spinning process are shown in Figures 11 and 12. Compared with the first two passes, in the third pass, the metal flow is stable. The maximum stresses at

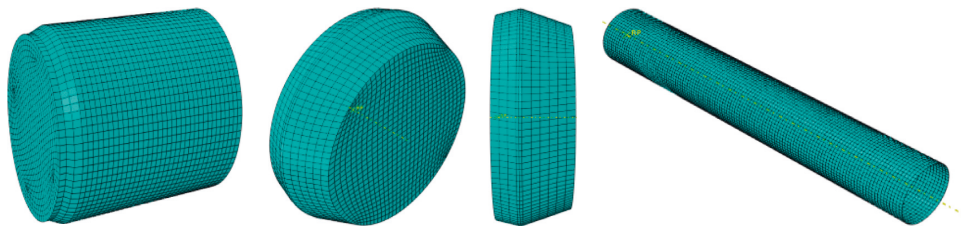

(a) (b) (c)

Figure 6: Simulation models. (a) Blank material model. (b) Spinning wheel models. (c) Mandrel model.

Table 4: Multipass numerical simulation spinning process parameters of magnesium alloy cylindrical parts.

Parameters	First pass	Second pass	Third pass	Fourth pass
Main spindle speed n (r/min)	60	60	90	60
Feed rate of the wheel f (mm/r)	1	1	0.7	0.7
Thinning rate of the wall φ_t (%)	23.3	26.1	29.4	25
Blank wall thickness t (mm)	30	23	17	12
Spinning temperature (°C)	270	270	270	270
Round corner diameter of the wheel r_p (mm)	10	10	10	10
Reduction of the rotating wheel C (mm)	6	6	3	3
Difference in reductions of the rotary wheels Δt (mm)	2	2	1	2

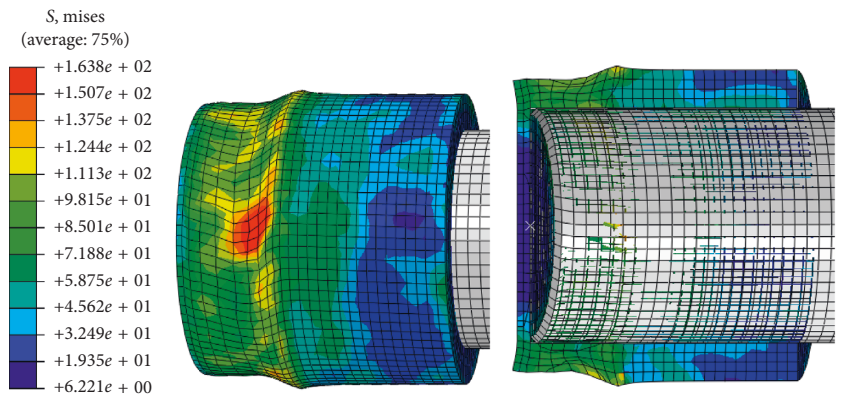

(a)

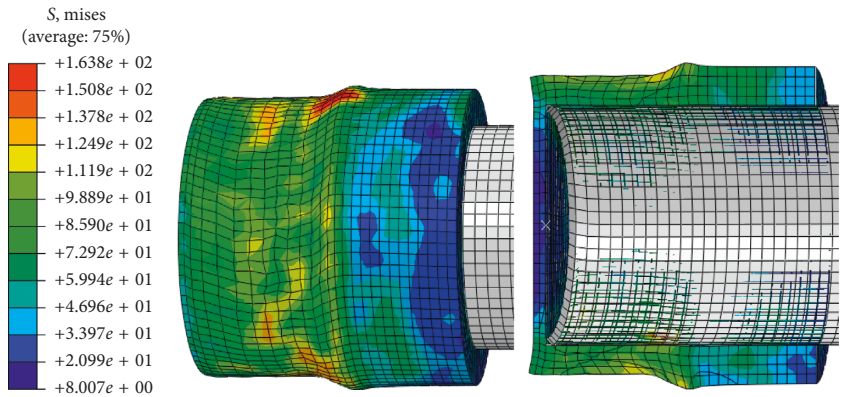

(b)

Figure 7: Continued.

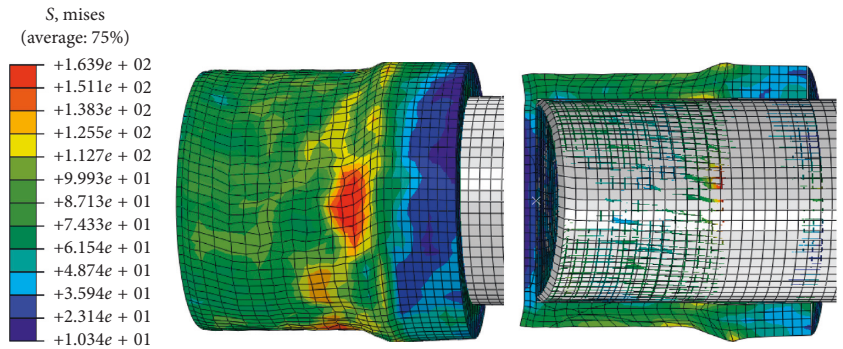

(c)

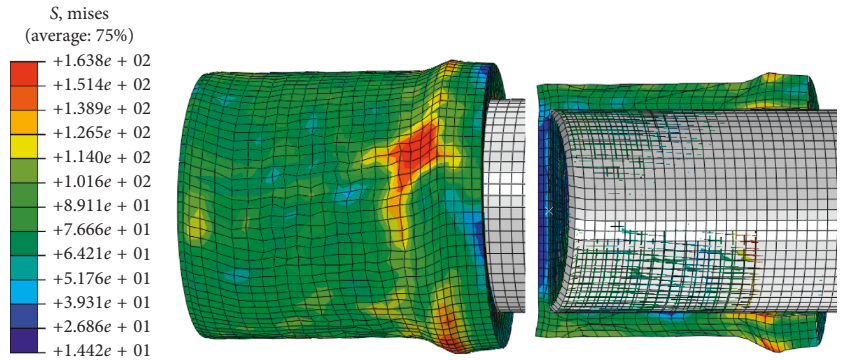

(d)

Figure 7: First-pass equivalent stress distribution. (a) 25%. (b) 50%. (c) 75%. (d) 100%.

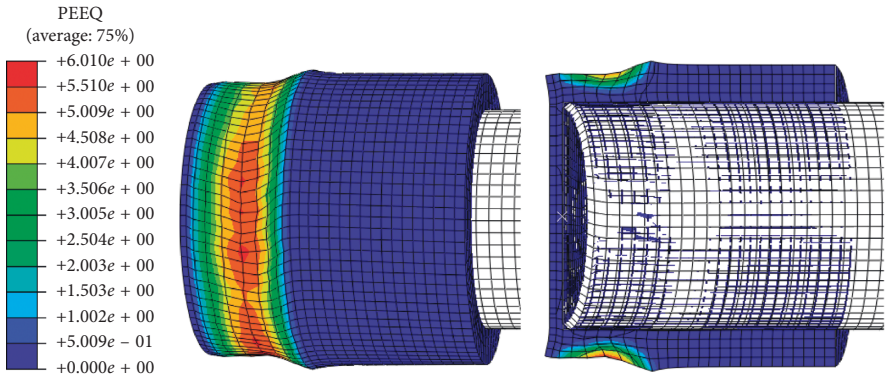

(a)

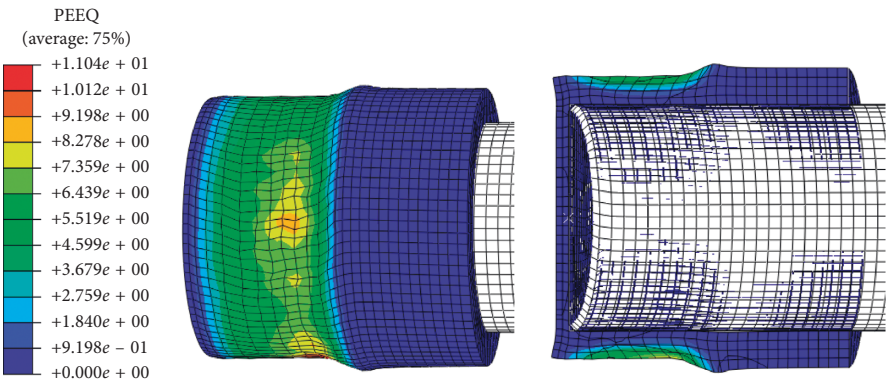

(b)

Figure 8: Continued.

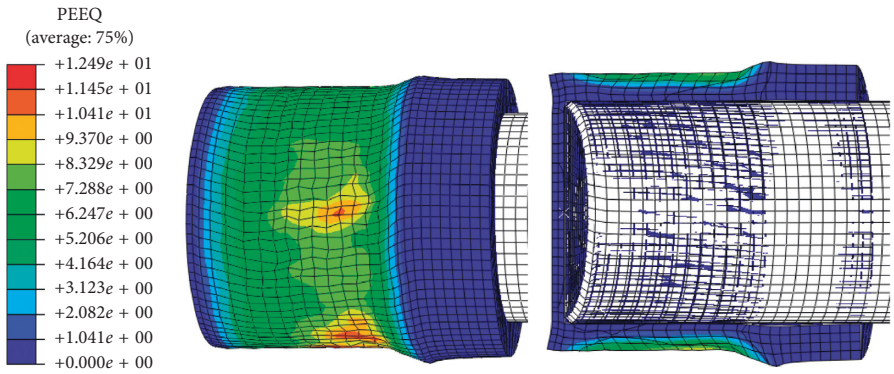

(c)

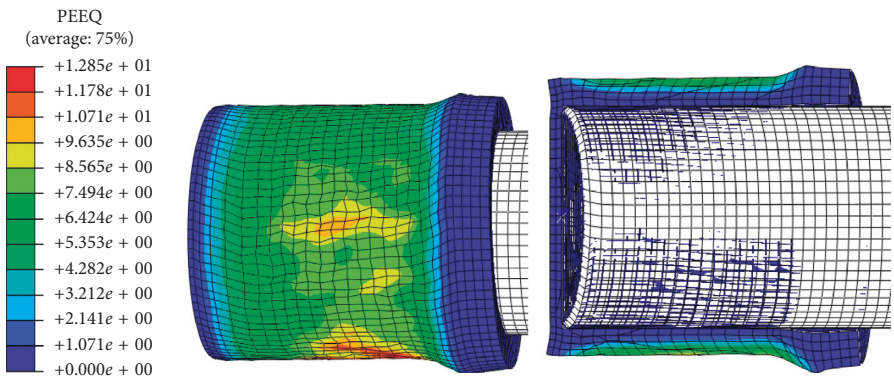

(d)

Figure 8: First-pass equivalent strain distribution. (a) 25%. (b) 50%. (c) 75%. (d) 100%.

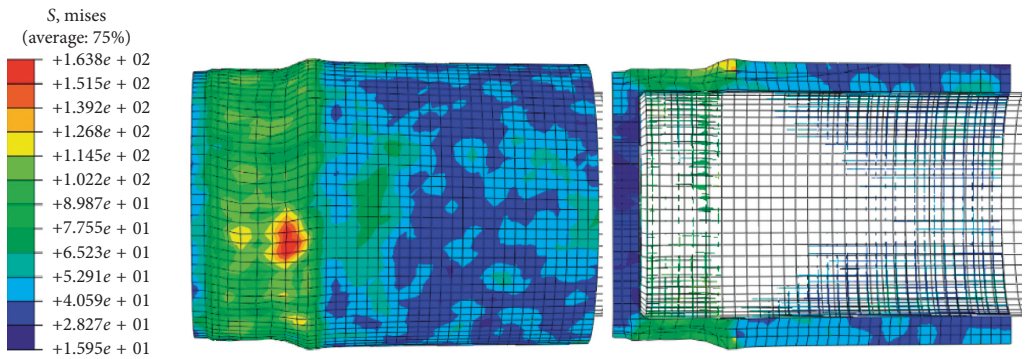

(a)

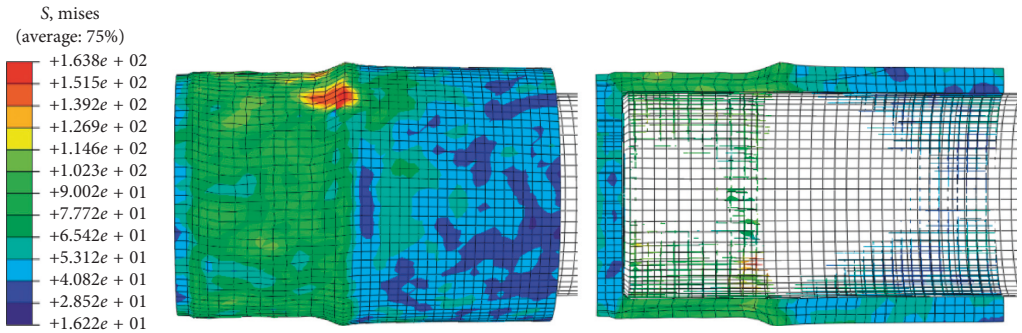

(b)

Figure 9: Continued.

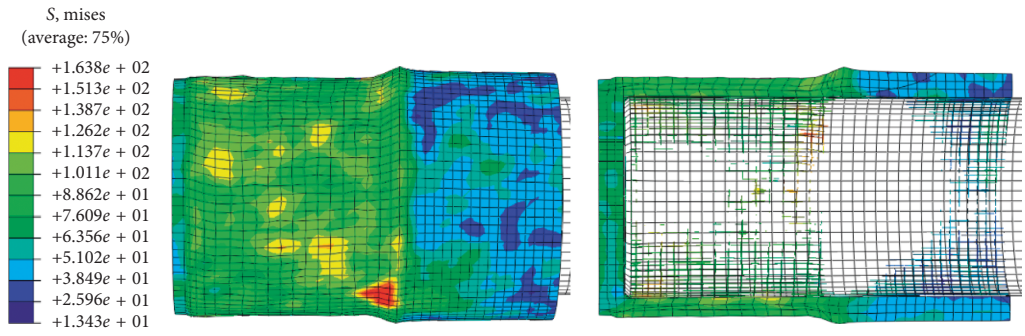

(c)

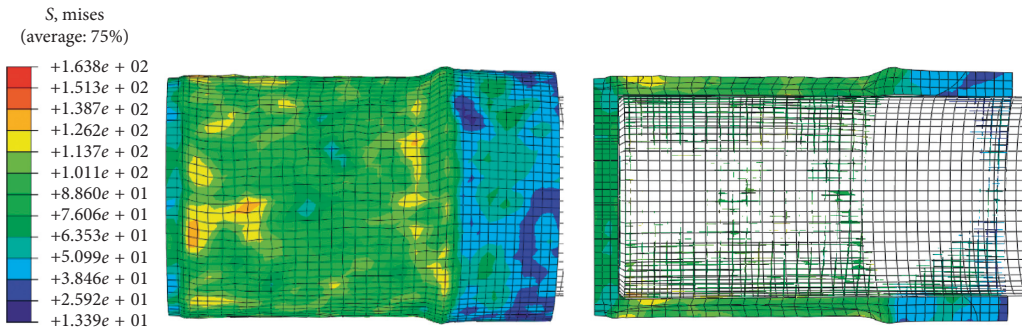

(d)

Figure 9: Second-pass equivalent stress distribution. (a) 25%. (b) 50%. (c) 75%. (d) 100%.

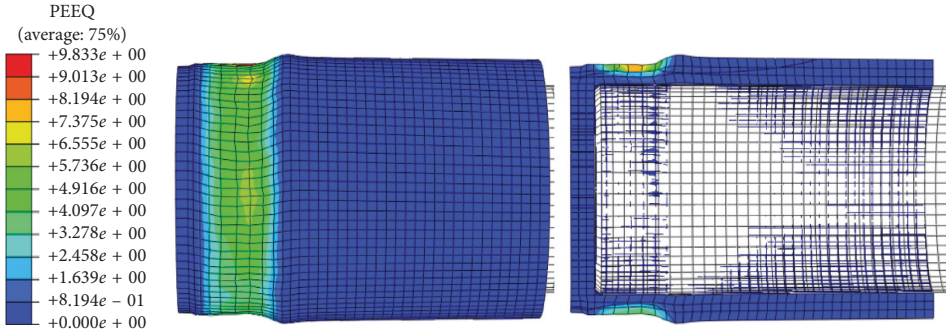

(a)

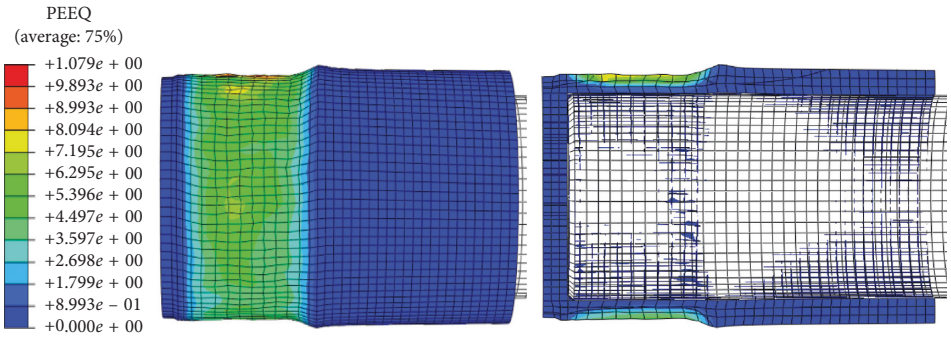

(b)

Figure 10: Continued.

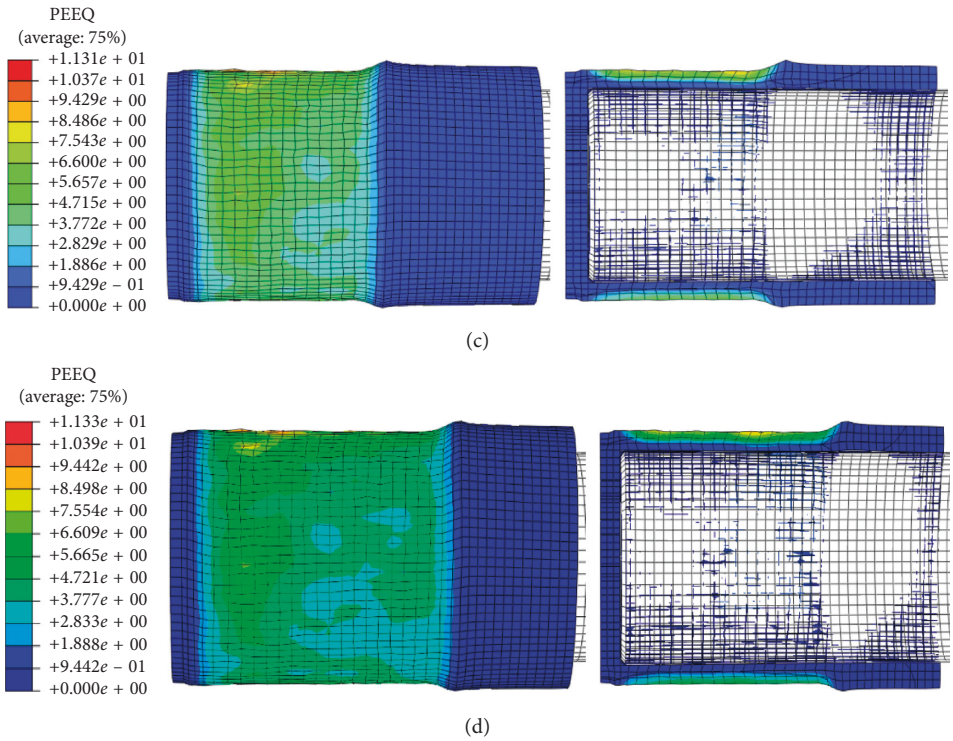

Figure 10: Second-pass equivalent strain distribution. (a) 25%. (b) 50%. (c) 75%. (d) 100%.

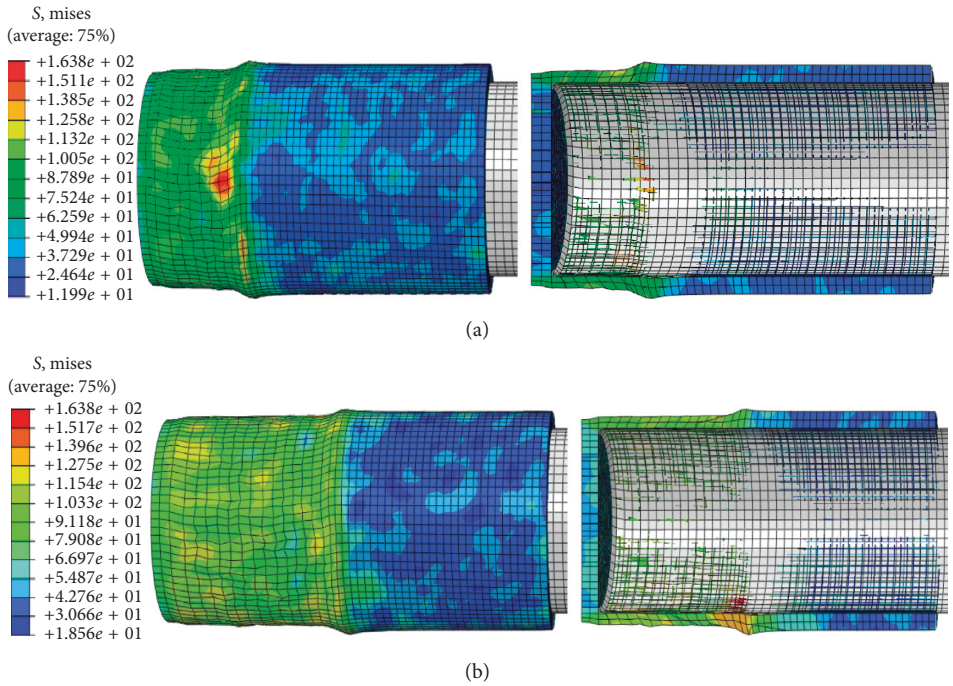

Figure 11: Continued.

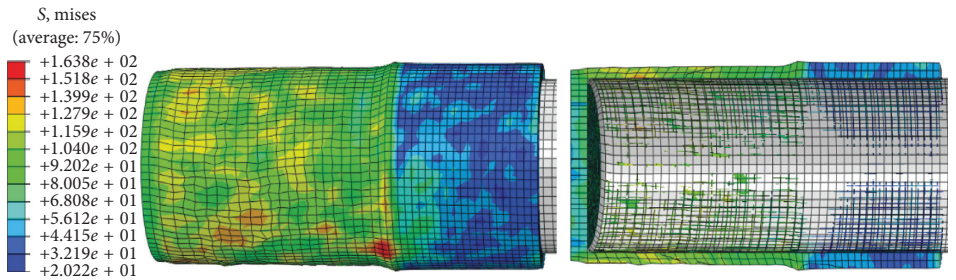

(c)

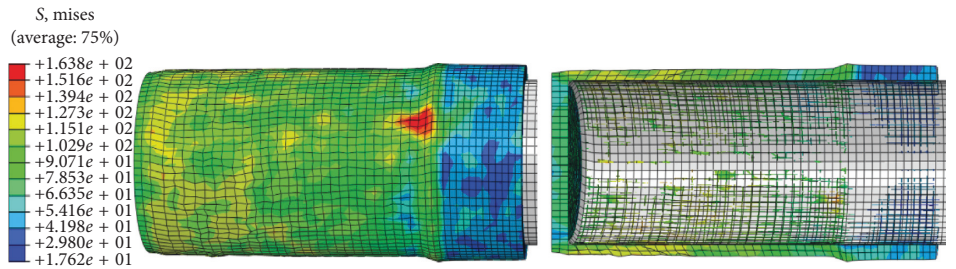

(d)

Figure 11: Third-pass equivalent stress distribution. (a) 25%. (b) 50%. (c) 75%. (d) 100%.

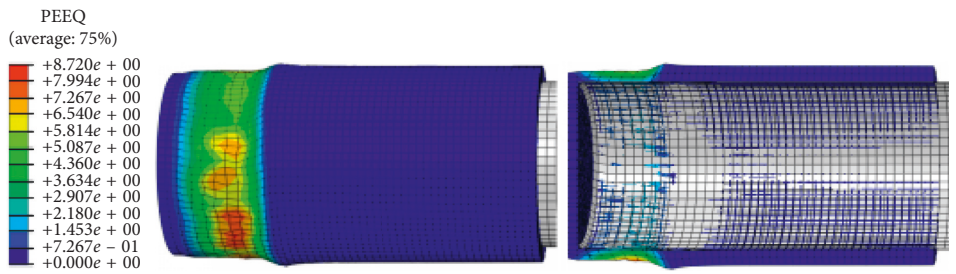

(a)

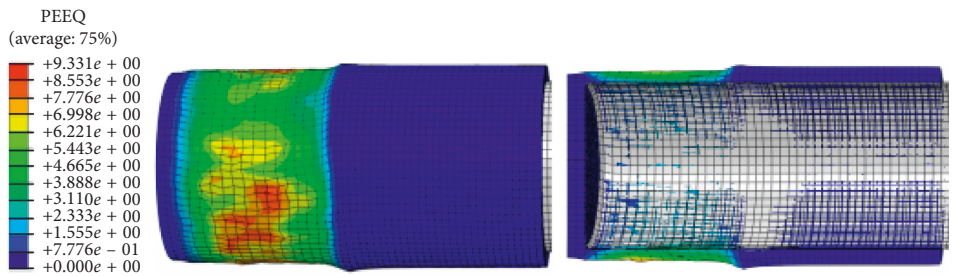

(b)

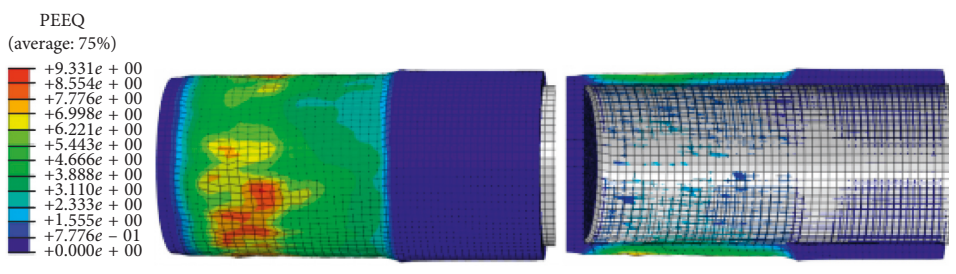

(c)

Figure 12: Continued.

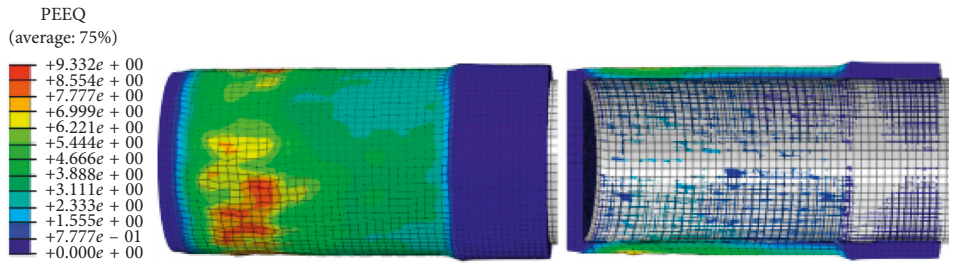

(d)

Figure 12: Third-pass equivalent strain distribution. (a) 25%. (b) 50%. (c) 75%. (d) 100%.

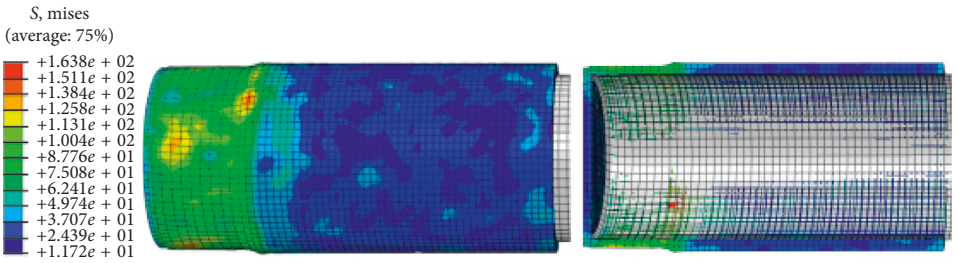

(a)

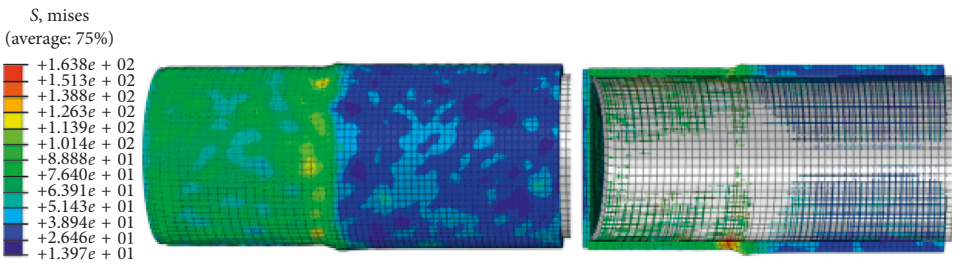

(b)

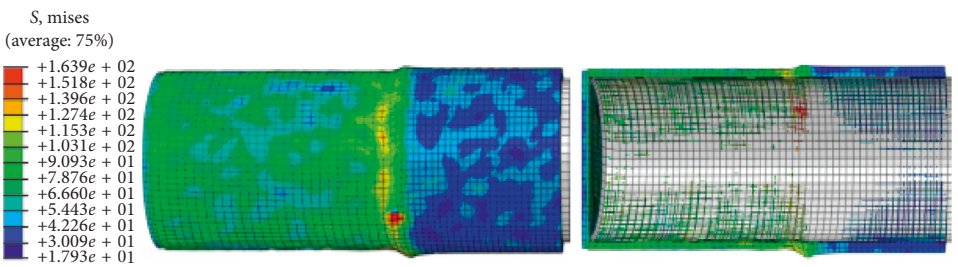

(c)

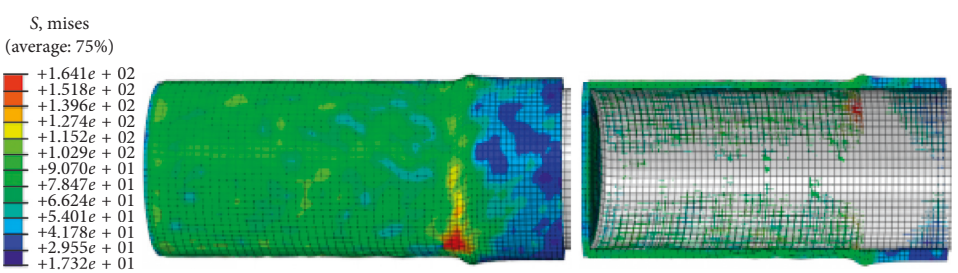

(d)

Figure 13: Fourth-pass equivalent stress distribution. (a) 25%. (b) 50%. (c) 75%. (d) 100%.

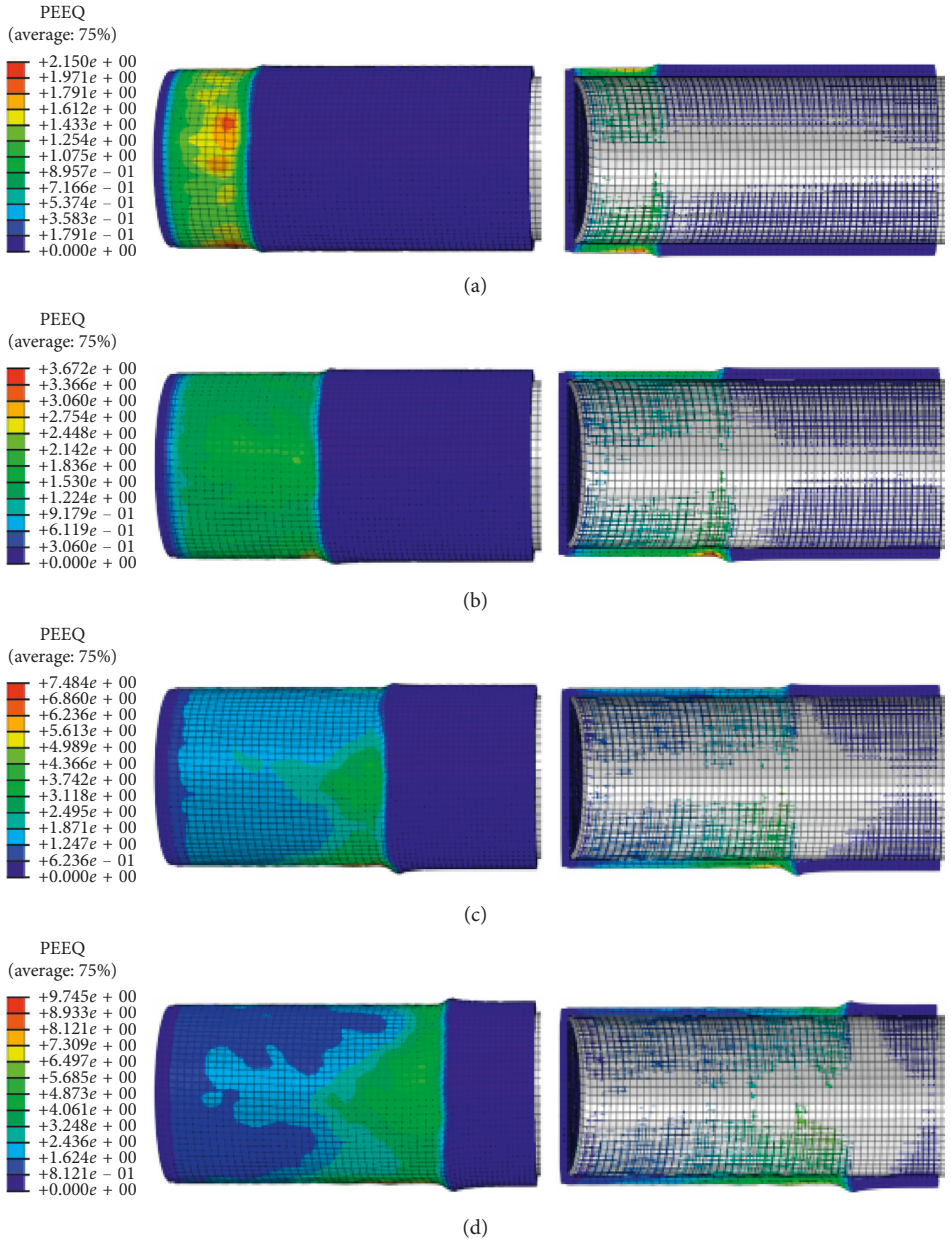

Figure 14: Fourth-pass equivalent strain distribution. (a) 25%. (b) 50%. (c) 75%. (d) 100%.

each pass are the same and at the contact point between the rotating wheel and the blank. The blank is well applied, while the end of it is parallel. The bottom of the blank is thinned.

The equivalent strain distribution of the third-pass spinning process is shown in Figure 12.

As can be seen from the Figure 12, the work piece is substantially "compressed," and the equivalent strain of the inner surface of the blank is smaller than that of the outer surface. The grid distortion in some areas occurs at 10%, but there is no influence on the subsequent spinning simulation, so the simulation results are available, and the difference in wall thickness will be compensated by the last pass.

2.3.4. Stress, Strain, and Cross-Sectional Distribution of the Fourth Pass. The stress, strain, and cross-sectional distribution of the fourth pass of the spinning process are shown in Figures 13 and 14. The fourth pass is the last pass in the spin forming. It can be seen from the cloud diagram that the metal flow is relatively stable during the forming process, and the maximum stress is at the contact point of the rotating wheel and the blank, which proves that the blank is well applied. However, a slight stacking phenomenon occurs at the end of the blank, and the bottom of it is thinned.

The equivalent strain distribution of the fourth-pass spinning process is shown in Figure 14.

Table 5: Modified process parameters.

Parameters	First pass	Second pass	Third pass	Fourth pass
Spindle speed n (r/min)	60	90	60	60
Feed rate of the rotary wheel f (mm/r)	1	0.7	1	0.7
Spinning temperature (°C)	270	270	270	270
Round corner diameter of the rotary wheel r_p (mm)	10	10	10	10
Reduction of the rotary wheel C (mm)	6	6	3	3
Difference in reduction of rotary wheels Δt (mm)	2	2	1	2

As can be seen from Figure 14, the work piece is completely pressed well, and the equivalent strain on the inner and outer surfaces of the blank is substantially the same. The equivalent strain peak appears in the second half, and the wall thickness is thinned in the second half where a wall thickness difference occurs in the circumferential direction. There is a slight stacking at the end of the blank.

2.3.5. Recommended Parameters for Forming Test. Through the simulation test of the spinning simulation data in Table 4, according to the stress-strain cloud diagram analysis in each pass forming process, the corresponding process test parameters are mainly modified for the spindle speed and the rotary feed rate to solve the prominent problems such as bulging and uneven wall thickness during the process. The modified process parameters are shown in Table 5, which are the practical parameters for the actual forming test.

3. Spinning Test of Cylindrical Magnesium Alloy Parts

3.1. Design and Manufacture of Magnesium Alloy Spinning Mold. The magnesium alloy shell parts are spun and formed in the two-wheel spinning machine, QX62-250 model, with the spinning pressure of 250 KN, the longitudinal stroke 1200 mm, and the lateral stroke 300 mm. Combined with the spinning machine capacity and sample technical indicators, the mold tooling is designed and processed. In this process, it is worth noting that the thermal expansion coefficient of magnesium alloy is 27×10^{-6}/°C, and the thermal expansion coefficient of the mold is 12×10^{-6}/°C. The influence of different thermal expansion rates on the forming is supposed to be considered in the hot-spin forming process. The precision of the spin forming is ensured by the design of the mold size and the spinning trajectory. According to the results of the numerical simulation analysis of the magnesium alloy cylindrical parts, the installation state of the spinning mandrel is shown in Figure 15, and the photo of the test blank is shown in Figure 16.

3.2. Spinning Test of Magnesium Alloy Shell Parts. Based on the research of numerical simulation, we carried out the spinning test of magnesium alloy tubular parts. Multipass spin forming was applied, and the spinning process parameters of magnesium alloy shell parts were tested with the spinning process parameters in Table 5. In the course of the experiment, we applied the propane-oxygen flame heating process, and the mandrel mold was uniformly heated by the rotation of the main shaft and heated by flame. During the heating process, we employed an infrared temperature measuring instrument to detect the temperature and stopped heating at 200°C.

Figure 15: Hot rotary core mold installation state.

Figure 16: Test blank material.

The magnesium alloy blank was assembled to the mandrel at room temperature, and the inside of the blank was coated with molybdenum disulfide as a lubricant. The mandrel was rotated by flame evenly. The temperature was monitored by an infrared thermometer and controlled in real time during the spinning process. When the temperature is lower, the flame increases; while the temperature is higher, the flame decreases or stays away from the blank.

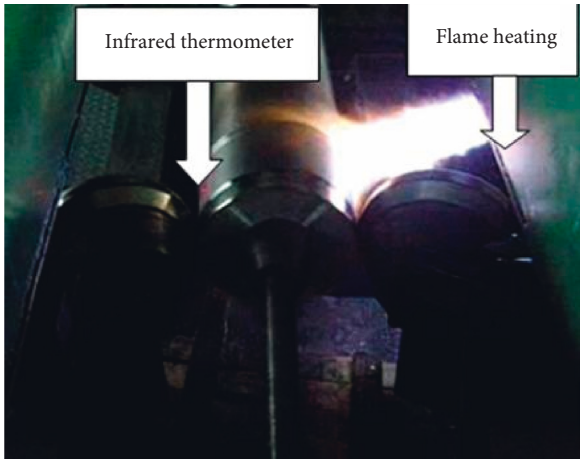

Figure 17: Temperature control and heating during spinning.

After many tests, it is found that the forming is very stable when the temperature is 280°C with the accuracy being ±5°C. The temperature control photo in the spinning process is shown in Figure 17.

3.3. Analysis of Spinning Defects. During the hot spinning test of the magnesium alloy, defects occurred in the first spinning peeling and the bottom fracture of the third spinning shell. Figure 18 shows the first spinning and peeling phenomenon. Figure 19 shows the fracture in the bottom of the shell in the third pass.

Such factors in spinning as the spinning temperature, the thinning rate, the feed rate, the hardness of the material, and the working angle of the rotating wheel are likely to cause material bulging and the peeling on the spinning surface. After analyzing the various process parameters of the magnesium alloy spinning test, we found that during the spinning process, the heating temperature control in the initial state of the spinning was unstable, and the surface temperature of the blank was too high, which resulted in a significant decrease in the hardness of the magnesium alloy and skin defects. There are two reasons for the analysis of the fracture defects in the third pass. The first point is that the third-pass reduction rate is too large. When the detonation rate is too large, there is a larger additional tensile stress in the inner wall of the spinner, which causes lateral cracks on the inner surface of the spinning member, and the spinning member may be fractured when the plastic deformation ability of the material exceeds. The second point is that the heating temperature does not remain stable, and the spinning temperature is too low when the thinning is too large.

3.4. Optimization and Experiment of Hot Spinning Process Parameters of Magnesium Alloy Shell Parts. We find that the spinning temperature and the thinning rate have a great influence on the spin forming of magnesium alloys. When the thinning rate is too high, the deformation rate of magnesium alloy is increased; when the thinning rate is too low, the surface temperature of the blank is high, which causes severe peeling and affects the quality of the finished

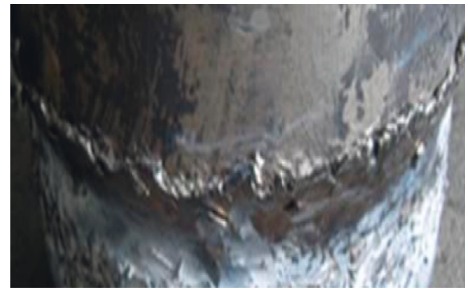

Figure 18: Spinning peeling defect.

Figure 19: Spinning fracture defect.

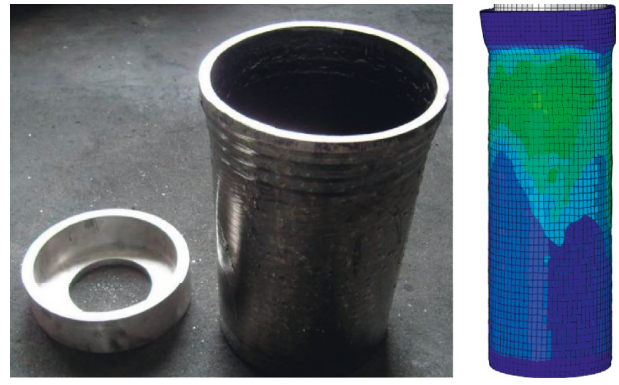

(a) (b)

Figure 20: Blank and finished sample product and numerical simulation.

product, as shown in Figure 18. When the temperature is low, it is easy to cause fracture, as shown in Figure 19. The relationship between the thinning rate and temperature is that when the thinning rate is high (more than 25%), the spinning temperature is higher and the control temperature is between 270–300°C; when the thinness rate is low (10–25%), the control temperature is between 260–270°C.

The desired target sample is spun by optimizing the temperature control and thinning rate in the first pass and the third pass. Figure 20 shows the blank, finished sample product, and the numerical simulation. Detailed experimental parameters are shown in Table 6.

The tensile properties of the spinning magnesium alloy sample shell were tested. The specimen was 165 mm long, 28 mm wide, and 5 mm thick. The effective stretch deformation section was 65 mm long, 5 mm wide, and 5 mm

Table 6: Final process parameters.

Parameters	First pass	Second pass	Third pass	Fourth pass
Spindle speed n (r/min)	60	90	60	60
Feed rate of the rotary wheel f (mm/r)	1	0.7	0.7	0.7
Thinning rate of the wall (theoretical value) φ_t (%)	23	26	29	25
Spinning temperature (°C)	260 ± 5	270 ± 5	290 ± 5	270 ± 5
Round corner diameter of the rotary wheel r_p (mm)	10	10	10	10
Reduction of the rotary wheel C (mm)	6	6	3	3
Difference in reduction of rotary wheels Δt (mm)	2	2	1	2

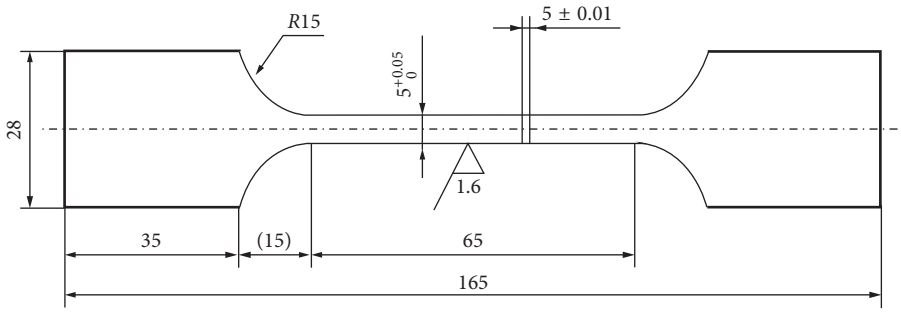

Figure 21: Test specimen design dimension.

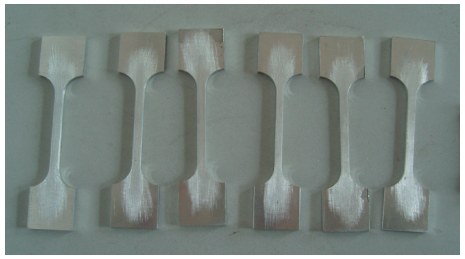

Figure 22: Performance of test specimens.

Table 7: Measurement and performance data of cylindrical magnesium alloy shell parts.

Number	Inside diameter (mm)	Outer diameter (mm)	Circumferential wall thickness difference (mm)	Intensity Rm (MPa)	Elongation A (%)
1	180.25	199.65	0.2	395	8.5
	180.13	199.45	0.2	385	9.2
2	180.20	199.62	0.2	390	8.9
	180.15	199.48	0.2	387	9.1

thick. The detailed size is shown in Figure 21, and the object of the performance test specimens is shown in Figure 22.

Table 7 shows the measured data of the finished magnesium alloy shell sample, which shows that the shell sample size and tolerance are within the expected target range. According to the tensile strength and elongation data, it is found that the strengthening and toughening effect of the magnesium alloy shell material after spinning is significant.

4. Conclusion

In this paper, the hot-spin forming technique, one of the advanced plastic forming techniques, combined with finite element numerical simulation analysis, was performed to study the hot-spin forming of cylindrical AZ80 magnesium alloy parts. The multipass hot-spin forming was simulated by ABAQUS software to help analyze the stress and strain distribution and changes during the spinning process and determine the test parameters for the actual spinning. Later, the setting of each parameter was optimized by the hot spinning test, especially the matching relationship between the parameters of temperature and the thinning rate. At last, the magnesium alloy cylindrical shell sample was finished.

Data Availability

The spinning process parameter data of magnesium alloys used to support the finding of this study are included within the article.

Conflicts of Interest

The authors declare that they have no conflicts of interest.

Acknowledgments

This research project was funded by the Science and Technology Development Plan of Jilin Province (project no. 20180201002G X).

References

[1] S. H. Zhang and Z. G. Wang, "Plastic processing technology of magnesium alloy," *Metal Forming Process*, vol. 21, no. 5, pp. 1–4, 2002.

[2] Q. X. Xia, S. Yuan, X. Q. Cheng, and G. F. Xiao, "Research status of hot spinning forming technology for magnesium alloys," *Forging Technology*, vol. 43, no. 7, pp. 103–111, 2002.

[3] L. L. Li, "Study on extrusion process of AZ31 magnesium alloy pipe," Master thesis, North University of China, Shanxi, China, 2006.

[4] Y. P. Zhang, J. Ai, and L. Jin, "Texture of rolled magnesium alloys and its control process," *Hot Working Process*, vol. 41, no. 11, pp. 116–118, 2012.

[5] I. R. Ahmad, X. Jing, and D. W. Shu, "Effect of temperature on the mechanical behaviour of magnesium alloy AZ91D in the range between −30°C and 250°C," *International Journal of Mechanical Sciences*, vol. 86, pp. 34–45, 2014.

[6] J. H. Kim, D. Y. Kim, Y. S. Lee et al., "A temperature-dependent elasto-plastic constitutive model for magnesium alloy AZ31 sheets," *International Journal of Plasticity*, vol. 50, pp. 116–118, 2013.

[7] Q. Xia, G. Xiao, H. Long, X. Cheng, and X. Sheng, "A review of process advancement of novel metal spinning," *International Journal of Machine Tools and Manufacture*, vol. 85, no. 7, pp. 100–121, 2014.

[8] P. C. Wang, Q. Y. Kawai, and Z. Y. Yue, "Magnesium alloy spinning technology in Japan," *Forging Technology*, vol. 33, no. 6, pp. 6–12, 2008.

[9] Z. Cao, "Study on the powerful spinning process of AZ80 magnesium alloy," Master thesis, Shanghai Jiaotong University, Shanghai, China, 2015.

[10] T. T. Zhang, W. X. Wang, X. Q. Cao et al., "Microstructure and micro-nano mechanical properties of magnesium alloy cylindrical parts by strong spinning," *Rare Metal Materials and Engineering*, vol. 47, no. 5, pp. 1573–1577, 2018.

[11] C. G. Wang, *Spinning Technology*, Machinery Industry Press, Beijing, China, 1986.

[12] Z. F. Sun and S. H. Wang, "Finite element numerical simulation of spinning of cylindrical parts," *Forging Technology*, vol. 37, no. 5, pp. 171–115, 2012.

[13] C. A. Zhang, C. M. Cheng, and R. Q. Li, "Spinning numerical simulation and process parameter optimization of cylindrical parts," *New Technology and Process*, vol. 7, pp. 104–107, 2010.

[14] T. Zhang, X. H. Li, J. Wei Jun et al., "Study on the influence of process parameters on spinning quality of thin-walled cylindrical parts with large diameter-thickness ratio," *Journal of Plastic Engineering*, vol. 24, no. 2, pp. 75–81, 2017.

[15] E. Yukutake, J. Kaneko, and M. Sugamata, "Anisotropy and non-uniformity in plastic behavior of AZ31 magnesium alloy plates," *Materials Transactions*, vol. 44, no. 4, pp. 452–457, 2003.

[16] H. Zhang, G. Huang, H. J. Roven, L. Wang, and F. Pan, "Influence of different rolling routes on the microstructure evolution and properties of AZ31 magnesium alloy sheets," *Materials & Design*, vol. 50, pp. 667–673, 2013.

[17] Y. X. Li, "Staggered spinning and its application," *Forging Technology*, vol. 13, no. 6, pp. 41–45, 1989.

[18] N. Zhang, W. Tan, Y. H. Li et al., "Numerical simulation and spinning pressure analysis of cylinder staggered spinning," *Journal of Shenyang University of Technology*, vol. 28, no. 5, pp. 55–58, 2009.

[19] C. J. Yang, "Study on microstructure properties and application of AZ61 and AZ80 magnesium alloys," Master thesis, Chongqing University, Chongqing, China, 2007.

[20] W. P. Qu and S. Gao, "Characteristics and application status of magnesium alloys," *Metal World*, vol. 2, no. 2, pp. 10–14, 2011.